A Natural Position Observer with Vertical Detection Coil for FSCW Machines

Ang Liu, Xiaoyan Huang, *Member*, *IEEE*, Zhuo Chen, Yelong Yu, Zhaokai Li, *Member*, *IEEE*, Jian Zhang

***Abstract*—This paper presents a sensorless control strategy using the novel detection coil for permanent magnet synchronous motor (PMSM) with fractional slot concentrated winding (FSCW). In order to eliminate the armature component in the coil voltage, the detection coil distribution is determined based on the analysis of synchronous inductance and leakage inductance for FSCW machines. Hence, the rotor position and angular velocity are estimated from the terminal voltage of detection coil, without any knowledge of motor parameters. Both finite element analysis (FEA) results and experiments are carried out to prove the effectiveness of the proposed method at steady and transient states.**

***Index Terms*—Detection coil, fractional slot concentrated windings, sensorless control.**

NOMENCLATURE

p_n	Number of pole-pairs
Z	Number of slots
θ_e	Rotor electrical position
ω_e	Rotor electrical angular speed
α_P	Slot-pitch angle
K_{dc}	Amplitude of permanent-magnet component in detection coil
M_s, M_l	Synchronous and leakage components of mutual inductance, respectively.
φ_r, φ_s, φ_t	Components of detection coil flux in *a-b-c* frame
u_r, u_s, u_t	Components of detection coil voltage in *a-b-c* frame
u_γ, u_δ	Components of detection coil voltage in α-β frame
θ_r, θ_s, θ_t	Angular difference to stator α axis of detection coil *r*, *s*, *t*.

I. INTRODUCTION

ROTOR position is essential for the field orientation control (FOC) of permanent-magnet synchronous motors (PMSM). During the past decades, various sensorless algorithms were designed for the estimation of rotor position θ_e and speed ω_e. Some estimators are based on the fact that θ_e or ω_e can be extracted from the motor model-based observers, e.g., sliding-mode observer [1] and extended Kalman filter [2]. Rotor saliency could also be used to estimate rotor position for interior PMSMs, in which high-frequency signals or current derivatives are measured to observe the rotor position [3], [4]. Considering the dependence on the motor parameters for those model-based estimators, online identification for single parameter is implemented in [5], [6]. However, the overall parameters cannot be easily obtained in the sensorless control due to rank deficiency.

Detection coils are introduced in the motor fault diagnosis [7], [8]. A position estimator based on detection coils is proposed in [9] for the fault-tolerant control application, which is independent from stator resistance. It is still one of model-based algorithm for the usage of mutual inductance and flux.

In order to avoid the parameter dependence and complexity of parameter tuning in existing position observers, this paper proposes a novel detection coil technique for sensorless control strategy in PMSM. The novel detection coil is investigated and designed in Section II and the mathematical model of detection coil is derived to extract the rotor position accordingly. The motor parameters show negligible influence on the extraction of rotor position. Finite element analysis (FEA) considering space vector pulse width modulation (SVPWM) is then carried out to verify the proposed method. Finally, the experimental results show a satisfactory compliance of the estimated position with the actual position without the knowledge of motor parameters (i.e., winding inductance and PM flux). With the proposed vertical detection coil, an online measurement of back electromotive force (EMF) in FSCW machines is offered for the estimation of rotor position. Then the EMF-based sensorless method could be extended to lower speed and higher load condition, which is the main contribution of this paper.

II. NOVEL DETECTION COIL DEMONSTRATION

The rotor position can be easily extracted with proper coil layout, as is the foundation of the proposed method. Generally, the flux linkage in a detection coil is described as the summation of armature component and permanent-magnet component in a three-phase machine. For the detection coil *r* located in the stator slots of phase A, the corresponding flux is expressed as:

$$\begin{aligned}\varphi_r &= \begin{bmatrix} M_{rA} & M_{rB} & M_{rC} \end{bmatrix} \begin{bmatrix} i_A & i_B & i_C \end{bmatrix}^T + K_{dc}\cos\left(\theta_e - \theta_r\right) \\ &= \begin{bmatrix} M_{srA}+M_{lrA} & M_{srB}+M_{lrB} & M_{srC}+M_{lrC} \end{bmatrix} \begin{bmatrix} i_A & i_B & i_C \end{bmatrix}^T \\ &\quad + K_{dc}\cos\left(\theta_e - \theta_r\right)\end{aligned} \quad (1)$$

where M_{rA}, M_{rB}, M_{rC} denote the inductances between the phase winding and detection coil, which consists of the synchronous and leakage inductance; i_A, i_B, i_C represent the stator currents; K_{dc} is the amplitude of permanent-magnet component in

This work was supported in part by the National Key R&D Program of China under Grant 2019YFE0123500, in part by the Zhejiang Provincial Ten-Thousand-Talent Plan under Grant 2019R52003, and in part by the Natural Science Foundation of China under grants U22A20214 and 51837010 *(Corresponding author: Jian Zhang).*

Ang Liu, Xiaoyan Huang, Zhuo Chen, Yelong Yu, Zhaokai Li and Jian Zhang are with the Zhejiang Provincial Key Laboratory of Electrical Machine Systems, College of Electrical Engineering, Zhejiang University, Hangzhou 310058, China (e-mail: a_liu@zju.edu.cn; xiaoyanhuang@zju.edu.cn; z.chen@zju.edu.cn; yuyelong@zju.edu.cn; zhaokai@kth.se; jian_zhang_zju@zju.edu.cn).

detection coil; θ_r is the angular position of detection coil r with the stator α axis.

A. Synchronous Inductance

According to the winding function, the synchronous inductance in FSCW motors is described as [10]

$$M_{sxy}=\frac{\mu_0 l_{ef} R_g}{g}\frac{16N_xN_y}{\pi}\sum_{v=1,odd}^{\infty}\frac{k_{xdv}k_{xpv}k_{ydv}k_{ypv}}{v^2}\cos\left[v\left(\theta_x-\theta_y\right)\right] \quad (2)$$

where μ_0 is the permeability in vacuum, l_{ef} is stack length, R_g is the air-gap radius, g is the air-gap length. v is the harmonic order. N_x, N_y, k_{xdv}, k_{ydv}, k_{xpv}, k_{ypv} are the turns, coil pitch factor and belt factor of coil x and coil y, respectively. θ_x and θ_y are the angular position of coil x and coil y with the stator α axis.

For M_{srA} in existing detection coil [9], the phase difference in (2) is equal to zero, whose axis is parallel with the corresponding stator phase, as shown in Fig. 1(a). The synchronous inductance of detection coil will vary linearly with the motor's and it is used for the position estimation.

Unlike the existing technique in [9], the novel detection coil distribution, namely vertical detection coil, is proposed to get rid of the parameter dependence. Two coils wound on contiguous stator teeth of the same phase are connected in reverse direction, as shown in Fig. 1 (b). The angular difference (θ_x-θ_y) is equal to 90° and therefore we have M_{srA}=0 for the vertical detection coil located in stator slots of phase A. Meanwhile, the synchronous inductance components between different phases (M_{rB} and M_{rC}) are much lower than that in the same phase (M_{srA}), which could be neglected safely [11].

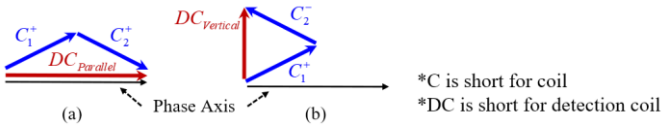

Fig. 1 Implantation of parallel and vertical detection coil.

B. Leakage Inductance

The slot leakage inductance is the main component of the leakage inductance between coil x and coil y and it is given as [12]

$$M_{lxy}=k_{xy}N_xN_yl_{ef}\lambda_{LS} \quad (3)$$

where k_{xy} is the leakage factor which is determined by the coil distribution and λ_{LS} is the slot permeance. More specifically, for the vertical detection coil located in phase A, the leakage factor can be divided into self-leakage factor, e.g. k_{rA}, and mutual-leakage factor, e.g. k_{rB} and k_{rC}.

For each single coil in stator slots, the self-leakage factors are the same. Therefore, the self-leakage component is eliminated in vertical detection coil due to the reverse connection.

As for mutual leakage inductance, it can be seen that the leakage flux always passes through the region within one-slot span which is shown in Fig. 2 (a). Therefore, the mutual leakage inductance is neglected in alternate tooth wound machines. For all teeth wound machines, coils 1~4 in Fig. 2 (b) will belong to the same phase if (4) is achieved

$$\alpha_P=\left|180^0-\frac{360^0\,p_n}{Z}\right|<\begin{cases}20^0 & 60^0 \text{ phase zone}\\ 40^0 & 120^0 \text{ phase zone}\end{cases} \quad (4)$$

where α_P is the slot-pitch angle. p, Z are the number of pole-pairs and slots, respectively. Then, the vertical detection coil can be located with coil 2 and coil 3 and the leakage flux produced by another phase winding will not be coupled into the detection coil. Therefore, mutual-leakage inductance factor is equal to zero under such circumstance.

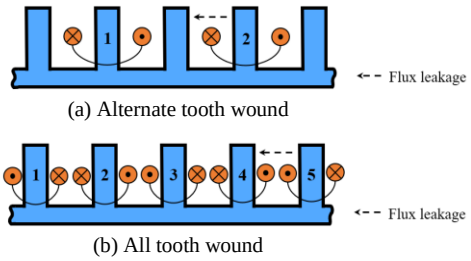

Fig. 2 Leakage flux path in alternate tooth and all tooth wound machines.

C. Vertical Detection Coil Configuration

From the above analysis, the armature component of flux linkage in vertical detection coil is compensated. It is worth emphasizing that the proposed method can be applied only when the slot-pole combination fulfills the condition in equation (4). Then the flux linkage of vertical detection coil is reduced to the permanent-magnet component:

$$\begin{bmatrix}\varphi_r\\ \varphi_s\\ \varphi_t\end{bmatrix}=K_{dc}\begin{bmatrix}\cos\left(\theta_e-\theta_r\right)\\ \cos\left(\theta_e-\theta_s\right)\\ \cos\left(\theta_e-\theta_t\right)\end{bmatrix}=K_{dc}\begin{bmatrix}\sin\theta_e\\ \sin\left(\theta_e-120^0\right)\\ \sin\left(\theta_e+120^0\right)\end{bmatrix} \quad (5)$$

where θ_r is equal to 90°. Without the knowledge of motor parameters, the mathematical model of coil terminal voltage in α-β axis is simplified as

$$\begin{bmatrix}u_\gamma & u_\delta\end{bmatrix}=\omega_eK_{dc}\begin{bmatrix}\cos\theta_e & \sin\theta_e\end{bmatrix} \quad (6)$$

D. Sensorless Control Strategy

The normalized phase-locked loop (PLL) in [13], [14] is adopted for the position estimation, for the purpose of performance improvement under various speeds. The diagram of normalized PLL is given in Fig. 3.

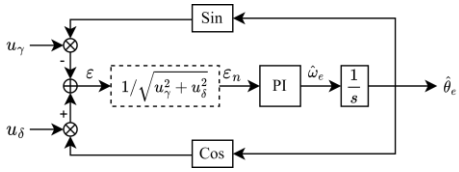

Fig. 3 Structure diagram of normalized PLL.

The block diagram of the hardware connection and software operation is presented in Fig. 4 (a). The differential amplification circuit is attached to the output of vertical detection coil before analog-to-digital conversion (ADC), as presented in Fig. 4 (b).

Then the output voltage achieves

$$\begin{aligned}u_o&=\frac{R_2+R_4}{R_1+R_3}\cdot\frac{R_3}{R_2}\cdot V_1-\frac{R_4}{R_2}\cdot V_2+\frac{R_2+R_4}{R_1+R_3}\cdot\frac{R_1}{R_2}\cdot V_{REF}\\&=\frac{R_4}{R_2}\cdot\left(V_1-V_2\right)+V_{REF}\end{aligned} \quad (7)$$

if we have R_1=R_2 and R_3=R_4. The operational amplifier TLV9062 is used in this letter and the resistors are chosen with 0.1% precision. Besides, the reference voltage V_{REF} is chosen as half of the maximum value ADC supports. The amplification and sample circuit will introduce acceptable cost to the system.

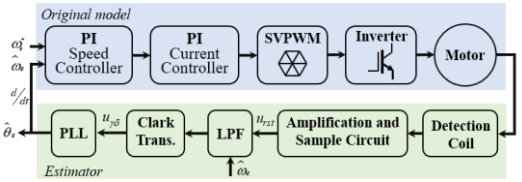

(a)

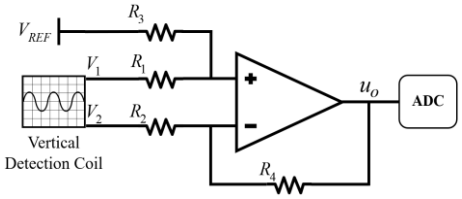

(b)

Fig. 4 (a) Block diagram of hardware and software (b) Amplification and sample circuit implementation

III. FEM Simulation and Experimental Verification

To validate the proposed method, an inverter-fed external-rotor PMSM (ER-PMSM) with double-layer concentrated winding is simulated using a commercial FEA software JMAG, as shown in Fig. 5 (a). Then the experimental results obtained from the test rig shown Fig. 6 are implemented to verify the proposed sensorless control approach. The main parameters of the 42-pole/36-slot motor are given in TABLE. I.

In order to minimize the impact to the stator slot filling factor, the detection coil wound around the stator teeth is only with 1 turn and the wire diameter is chosen as 0.3mm. The space occupied by detection coil is calculated as 0.07mm^2 in a stator slot larger than 50mm^2. The motor slot filling factor rose to 32.44% with the detection coil from 32.3%, thus the space occupied by detection coil can be ignored fairly.

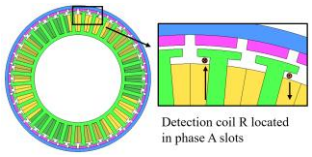

(a) FEA model

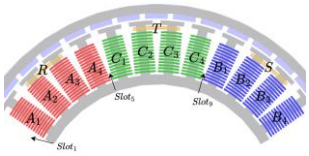

(b) Cross-sectional diagram

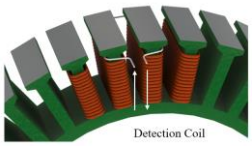

(c) 3D-CAD model of phase A

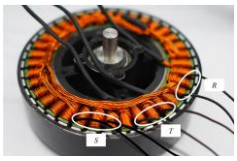

(d) Prototype

Fig. 5 Detection coil implementation in a 36-slot/42-pole machine.

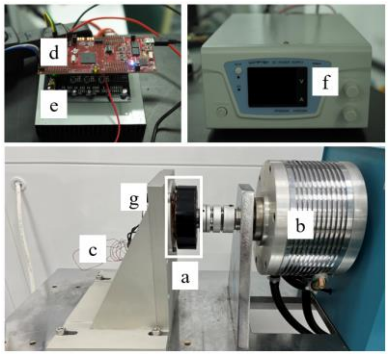

Fig. 6 The experimental setup (a) Prototype (b) Dynamometer (c) Detection coil (d) DSP control board (e) Voltage inverter (f) DC power supply (g) Encoder.

TABLE. I
Parameters of the Tested ER-PMSM

Parameter	Value	Parameter	Value
Vdc	36V	Flux linkage	4.5mWb
R	53mΩ	*L*	90uH
Rated speed	1500rpm	Rated current	5A
Winding connection	Star	Switch frequency	12kHz
Outer diameter	100mm	Effective length	20mm
Inner diameter	60mm	Airgap	0.5mm
Stator material	20JNEH1200	Rotor material	SCM420
Magnet	N38H	Pole-arc	0.71

A. Simulation Results

In order to intuitively present the influence of winding current on the detection coil, the permanent magnet is removed from the FEA model. It can be seen that, the terminal voltage of vertical detection is equal to zero, while there is a corresponding sinusoidal voltage in parallel detection coil with three-phase sinusoidal current excitation.

The simulation waveforms at rated load condition of parallel and vertical detection coils are given in Fig. 7. It demonstrates that the proposed detection coil distribution could effectively eliminate the current component in coil terminal voltage, thus, the sinusoidal permanent magnet component is extracted to estimate the rotor angular position. In contrast, the traditional approach with parallel detection coil exhibits heavy switching noise caused by current derivatives.

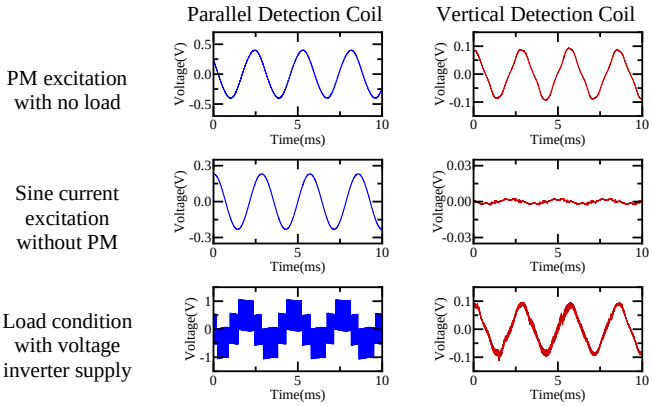

Fig. 7 Calculated voltage of detection coil in FEA simulation at rated speed.

Moreover, the FEA results under open circuit and load condition are presented in Fig. 8 which proves that, both the induced back-EMF and electromagnetic torque keep the same with/without the detection coil. In fact, the current flowing into the detection coil could be very small due to the high input impedance of the amplification and sample circuit [7]. Then the extra MMF caused by detection coil could be ignorable compared with the MMF of stator winding. Therefore, the integration of vertical detection coil will not affect the electromagnetic performance of the prototype.

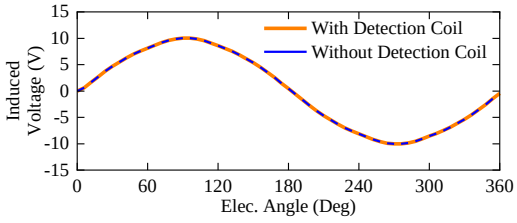

(a) Open circuit

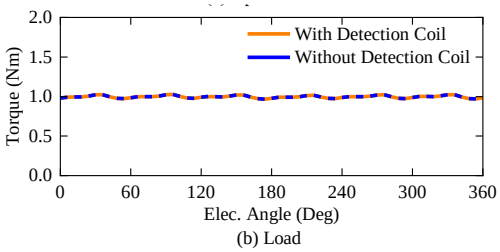

(b) Load

Fig. 8 FEA results with/without the detection coil.

B. Experimental performance at steady state

An incremental encoder of 3600 pulses per revolution (ppr) is assembled concentrically with the test motor for reference, as shown in Fig. 6. With the quadrature QEP module in DSP, the maximum value of potential electrical error for the 42-pole machine is less than 0.01 rad. When the ER-PMSM is operating, the detection coil voltage is sent into ADC ports of DSP (TI 28379D) control board after amplifying.

The experimental waveform of detection coil voltage under 1000 rpm is shown in Fig. 9, as well as the phase current. It is observed that the phase current derivatives in stator winding cause barely no ripple in detection coil. The estimated position shows satisfactory compliance with the real position from the encoder. Experimental results demonstrate that the maximum position error is less than 0.05rad(<3deg) with a 42-pole PM rotor, which means the mechanical error is less than 0.0025rad((<0.15deg).

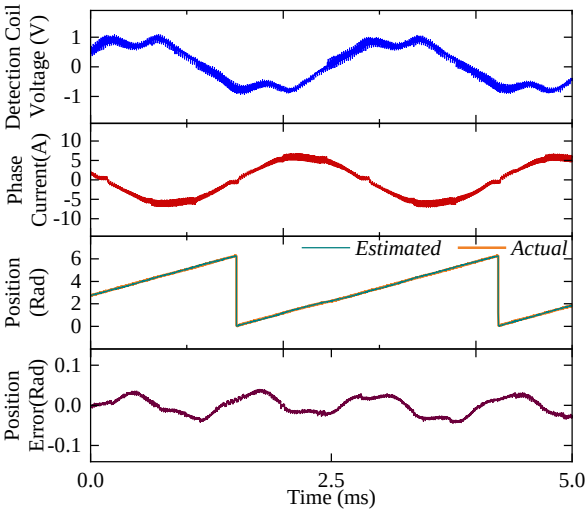

Fig. 9 The experimental results of the proposed sensorless control strategy.

Moreover, the position estimation errors under various speed/torque conditions are shown in TABLE. II and TABLE. III correspondingly as further validation. It can be seen that the maximum error keeps almost the same which proves the fact that the proposed method can be applied to various conditions.

TABLE. II
DETECTION ERRORS UNDER DIFFERENT SPEED COMMANDS (i_q=5A)

Motor Speed (Rpm)	500	1000	1500
Maximum **electrical** position error (Rad)	5.45e-2	4.85e-2	4.77e-2

TABLE. III
Detection Errors under Different Load Conditions (n =500rpm)

q-axis current (A)	5	10	15
Maximum **electrical** position error (Rad)	5.45e-2	5.72e-2	6.05e-2

C. Low Speed Performance

It is well known that the EMF-based sensorless strategy is not suitable for the low-speed operation, due to low signal-to-noise ratio (SNR). With the direct measurement of back-EMF signal via vertical detection coil, the proposed method achieves operation under 50rpm (<5% rated speed). Experimental results are given in Fig. 10, in which the maximum electrical position error is about 0.08 rad with the 10A phase current.

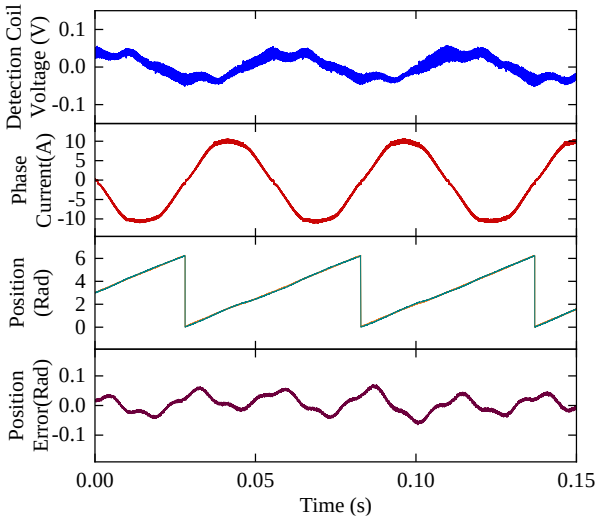

Fig. 10 The experimental results under 50 rpm.

D. Dynamic Performance

The prototype embedded with vertical detection coil firstly starts up using the I/f control strategy [15][16], as presented in Fig. 11. When the rotor speed reaches about 50rpm at which the estimated position is proved to achieve sufficient precision, the position signal used in current-loop controller is smoothly transited to the estimated value by the proposed strategy [17]. Finally, the field-oriented control with both speed and current close-loop controller is achieved and the rotor is accelerated to 500rpm.

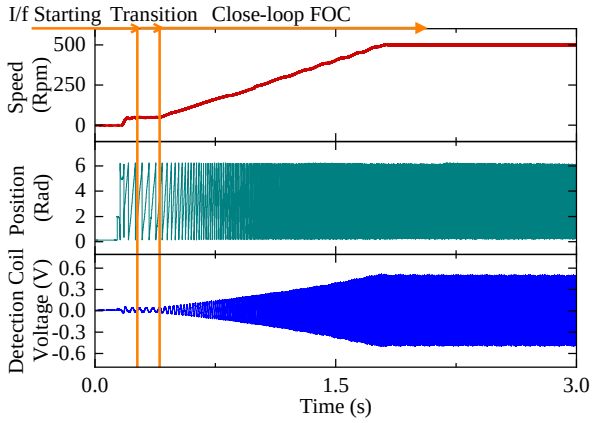

Fig. 11 Experimental results of startup process.

In Fig. 12, the speed command of test motor is initially set at 500rpm and then is accelerated to 1000rpm. The position error in the whole acceleration process is small to achieve great transient performance. And the maximum error is reduced when the rotor speed increases.

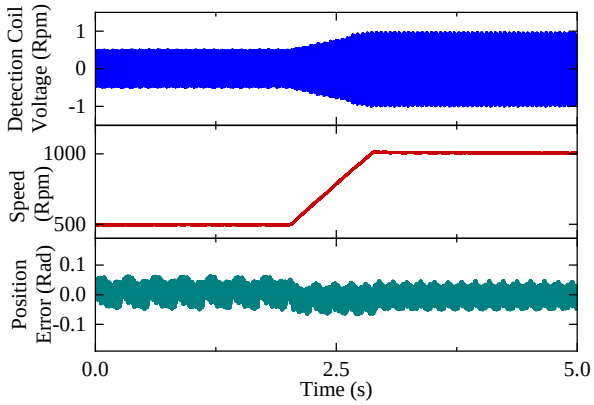

Fig. 12 The experimental results of acceleration.

As for load variation, Fig. 13 shows the position estimation results when the motor load is set to 2.0 Nm from 1.0 Nm under 50rpm. The maximum position error stays almost the same while the amplitude of phase current increased to 10 A. Experimental results verified the analytical conclusion that the influence of armature component to detection coil voltage is eliminated.

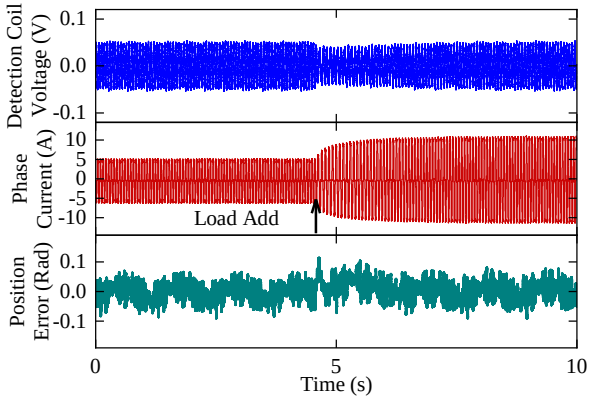

Fig. 13 Load transient performance under 50rpm.

E. Comparative Studies to Existing Methods

TABLE. IV states the comparison with existing techniques, in which the items of data set, required motor parameters, performance under different speeds, system cost and application range are presented. As a matter of fact, motor parameters including resistance and inductance are necessary for sliding-mode observer (SMO) and other existing techniques, while the proposed strategy based on vertical detection coil achieves totally parameter independence which means the parameter mismatch will show no disturbance.

Sliding mode observer [18] performs well in the middle/high speed range. However, the position error will increase for a relatively low speed (<5% rated speed) with rated load, as shown in Fig. 13. With the online measurement of back-EMF by vertical detection coil, the proposed method keeps high accuracy in such condition. The full-order observer could achieve comparable performance as ours under low-speed range [19]. Nevertheless, the design process is not easy since there are three free coefficients need to be tuned and the drive inertia is necessary. The inaccuracy of motor parameters will also affect the estimated position to some context.

Finally, it should be emphasized that, this method is still limited to FSCW machines, while the existing methods could be applied to all the PMSMs with better generalizability and no additional cost is needed.

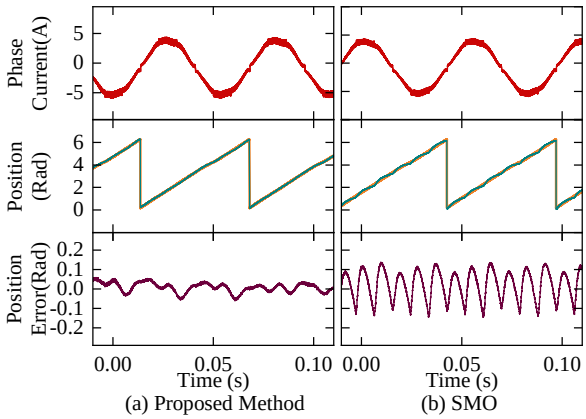

(a) Proposed Method (b) SMO

Fig. 14 Comparison with sliding-mode observer under 50 rpm.

TABLE. IV
Comparison with Existing Technique

	Proposed method with vertical detection coil	Existing method with parallel detection coil [9]	Sliding-mode observer [18]	Adaptive full-order observer [19]
Data set	Detection coil terminal voltages in α-β axis	Stator currents and detection coil terminal voltages in d-q axis	Stator voltages and currents in α-β axis	Stator voltages and currents in d-q axis
Required motor parameters	None	Mutual inductance, back-EMF constant of detection coil	Stator resistance and inductance	Stator resistance and inductance, drive inertia
Performance	Estimation accuracy almost stays the same under different speeds and loads	Maximum error less than 0.15 rad	Performs well under middle and high speed but not well for low speed	Performs well above 100rpm with proper feedback gain
System cost	Amplification circuits and detection coils that introduce acceptable cost	Data acquisition system and detection coils	No additional cost	No additional cost
Application range	FSCW machines achieving (4)	All the PMSMs	All the PMSMs	All the PMSMs

IV. Conclusion

This paper proposes an improved sensorless control strategy with novel detection coil technique to eliminate the influence of winding current in FSCW machines. The detection coil voltage vector is perpendicular to the corresponding phase axis with regard to the winding layout. An online measurement of back electromotive force is offered for the estimation of rotor position. The proposed sensorless control method is completely parameter independent and achieve well performance with an acceptable additional cost. Both FEM simulation considering PWM effect and experimental results under various conditions

have verified the proposed method. It should be noted that, the proposed method is limited to FSCW machines, and a wider application will be our future investigation.

V. References

[1] H. Kim, J. Son, and J. Lee, "A High-Speed Sliding-Mode Observer for the Sensorless Speed Control of a PMSM," *IEEE Transactions on Industrial Electronics*, vol. 58, no. 9, pp. 4069–4077, Sep. 2011, doi: 10.1109/TIE.2010.2098357.

[2] S. Bolognani, L. Tubiana, and M. Zigliotto, "Extended Kalman filter tuning in sensorless PMSM drives," *IEEE Transactions on Industry Applications*, vol. 39, no. 6, pp. 1741–1747, 2003, doi: 10.1109/TIA.2003.818991.

[3] J.-H. Jang, S.-K. Sul, J.-I. Ha, K. Ide, and M. Sawamura, "Sensorless drive of surface-mounted permanent-magnet motor by high-frequency signal injection based on magnetic saliency," *IEEE Transactions on Industry Applications*, vol. 39, no. 4, pp. 1031–1039, Jul. 2003, doi: 10.1109/TIA.2003.813734.

[4] M. X. Bui, D. Guan, D. Xiao, and M. F. Rahman, "A Modified Sensorless Control Scheme for Interior Permanent Magnet Synchronous Motor Over Zero to Rated Speed Range Using Current Derivative Measurements," *IEEE Transactions on Industrial Electronics*, vol. 66, no. 1, pp. 102–113, 2019, doi: 10.1109/TIE.2018.2823663.

[5] M. Rashed, P. F. A. MacConnell, A. F. Stronach, and P. Acarnley, "Sensorless Indirect-Rotor-Field-Orientation Speed Control of a Permanent-Magnet Synchronous Motor With Stator-Resistance Estimation," *IEEE Transactions on Industrial Electronics*, vol. 54, no. 3, pp. 1664–1675, Jun. 2007, doi: 10.1109/TIE.2007.895136.

[6] Y. Shi, K. Sun, L. Huang, and Y. Li, "Online Identification of Permanent Magnet Flux Based on Extended Kalman Filter for IPMSM Drive With Position Sensorless Control," *IEEE Transactions on Industrial Electronics*, vol. 59, no. 11, pp. 4169–4178, 2012, doi: 10.1109/TIE.2011.2168792.

[7] Y. Da, X. Shi, and M. Krishnamurthy, "A New Approach to Fault Diagnostics for Permanent Magnet Synchronous Machines Using Electromagnetic Signature Analysis," *IEEE Transactions on Power Electronics*, vol. 28, no. 8, pp. 4104–4112, 2013, doi: 10.1109/TPEL.2012.2227808.

[8] K.-T. Kim, S.-T. Lee, and J. Hur, "Diagnosis Technique Using a Detection Coil in BLDC Motors With Interturn Faults," *IEEE Transactions on Magnetics*, vol. 50, no. 2, pp. 885–888, 2014, doi: 10.1109/TMAG.2013.2282152.

[9] Y. Da, X. Shi, and M. Krishnamurthy, "A Novel Universal Sensor Concept for Survivable PMSM Drives," *IEEE Transactions on Power Electronics*, vol. 28, no. 12, pp. 5630–5638, 2013, doi: 10.1109/TPEL.2013.2252198.

[10] R. Krall, J. Krenn, and A. Schmid, "Fractional slot winding versus distributed winding using winding function method," in *2014 International Conference on Optimization of Electrical and Electronic Equipment (OPTIM)*, 2014, pp. 437–444. doi: 10.1109/OPTIM.2014.6850900.

[11] A. M. El-Refaie, Z. Q. Zhu, T. M. Jahns, and D. Howe, "Winding Inductances of Fractional Slot Surface-Mounted Permanent Magnet Brushless Machines," in *2008 IEEE Industry Applications Society Annual Meeting*, 2008, pp. 1–8. doi: 10.1109/08IAS.2008.61.

[12] R. Dutta, M. F. Rahman, and L. Chong, "Winding Inductances of an Interior Permanent Magnet (IPM) Machine With Fractional Slot Concentrated Winding," *IEEE Transactions on Magnetics*, vol. 48, no. 12, pp. 4842–4849, 2012, doi: 10.1109/TMAG.2012.2203140.

[13] Q. An, J. Zhang, Q. An, X. Liu, A. Shamekov, and K. Bi, "Frequency-Adaptive Complex-Coefficient Filter-Based Enhanced Sliding Mode Observer for Sensorless Control of Permanent Magnet Synchronous Motor Drives," *IEEE Transactions on Industry Applications*, vol. 56, no. 1, pp. 335–343, Jan. 2020, doi: 10.1109/TIA.2019.2951760.

[14] Z. Xu, T. Zhang, Y. Bao, H. Zhang, and C. Gerada, "A Nonlinear Extended State Observer for Rotor Position and Speed Estimation for Sensorless IPMSM Drives," *IEEE Transactions on Power Electronics*, vol. 35, no. 1, pp. 733–743, Jan. 2020, doi: 10.1109/tpel.2019.2914119.

[15] S. Ye and X. Yao, "An Enhanced SMO-Based Permanent-Magnet Synchronous Machine Sensorless Drive Scheme With Current Measurement Error Compensation," *IEEE Journal of Emerging and Selected Topics in Power Electronics*, vol. 9, no. 4, pp. 4407–4419, Aug. 2021, doi: 10.1109/JESTPE.2020.3038859.

[16] M. Pacha and S. Zossak, "Improved Simple I-F Open-Loop Start-up of PMSM Drives Without Speed or Position Sensor," in *2019 IEEE 10th International Symposium on Sensorless Control for Electrical Drives (SLED)*, Sep. 2019, pp. 1–6. doi: 10.1109/SLED.2019.8896231.

[17] M. Fatu, R. Teodorescu, I. Boldea, G.-D. Andreescu, and F. Blaabjerg, "I-F starting method with smooth transition to EMF based motion-sensorless vector control of PM synchronous motor/generator," in *2008 IEEE Power Electronics Specialists Conference*, Jun. 2008, pp. 1481–1487. doi: 10.1109/PESC.2008.4592146.

[18] C. Gong, Y. Hu, J. Gao, Y. Wang, and L. Yan, "An Improved Delay-Suppressed Sliding-Mode Observer for Sensorless Vector-Controlled PMSM," *IEEE Transactions on Industrial Electronics*, vol. 67, no. 7, pp. 5913–5923, Jul. 2020, doi: 10.1109/TIE.2019.2952824.

[19] S. Po-ngam and S. Sangwongwanich, "Stability and Dynamic Performance Improvement of Adaptive Full-Order Observers for Sensorless PMSM Drive," *IEEE Transactions on Power Electronics*, vol. 27, no. 2, pp. 588-600, Feb. 2012, doi: 10.1109/TPEL.2011.2153212.